SCIENTIFIC REPORTS
natureresearch

OPEN

Transport Properties and Finite Size Effects in β-Ga_2O_3 Thin Films

Robin Ahrling[1], Johannes Boy[1], Martin Handwerg[1], Olivio Chiatti[1], Rüdiger Mitdank[1], Günter Wagner[2], Zbigniew Galazka[2] & Saskia F. Fischer[1]

Received: 1 October 2018
Accepted: 21 August 2019
Published online: 11 September 2019

Thin films of the wide band gap semiconductor β-Ga_2O_3 have a high potential for applications in transparent electronics and high power devices. However, the role of interfaces remains to be explored. Here, we report on fundamental limits of transport properties in thin films. The conductivities, Hall densities and mobilities in thin homoepitaxially MOVPE grown (100)-orientated β-Ga_2O_3 films were measured as a function of temperature and film thickness. At room temperature, the electron mobilities ((115 ± 10) cm^2/Vs) in thicker films (>150 nm) are comparable to the best of bulk. However, the mobility is strongly reduced by more than two orders of magnitude with decreasing film thickness ((5.5 ± 0.5) cm^2/Vs for a 28 nm thin film). We find that the commonly applied classical Fuchs-Sondheimer model does not explain sufficiently the contribution of electron scattering at the film surfaces. Instead, by applying an electron wave model by Bergmann, a contribution to the mobility suppression due to the large de Broglie wavelength in β-Ga_2O_3 is proposed as a limiting quantum mechanical size effect.

Over the past years, gallium oxide (Ga_2O_3) has proved to be a promising candidate for a variety of possible applications, such as deep UV-detectors, gas sensors, but especially for high power devices[1–4]. Gallium oxide is a transparent semiconductor with a high band gap of 4.7 to 4.9 eV at room temperature[5–8], which exceeds that of other common wide band gap materials (3.2 eV for SiC, 3.3 eV for GaN[9]). The β-form of Ga_2O_3 is most commonly used, since it can be grown from melt and is the most stable configuration. However, to date fundamental material properties in particular for thin films[10,11] are under investigation.

So far, only n-type conductivity has been observed in β-Ga_2O_3. The effective mass has been reported to be 0.25–0.28 electron masses[12–14]. Various temperature-dependent measurements of electrical parameters on bulk single-crystals, typically grown by the Czochralski-method, have been done before, with the highest mobilities measured in comparable bulk material (Hall densities of about some $10^{17}\,cm^{-3}$) so far being 152 $\frac{cm^2}{Vs}$[15]. With the progress made in the production of homoepitaxial β-Ga_2O_3 thin films of high quality[16], they have a promising prospect for potential use in devices. However, to date, the temperature and film thickness dependence of the electrical behavior of thin films remains largely unknown.

In this work, thin homoepitaxially metal-organic vapour phase epitaxy (MOVPE) grown (100) β-Ga_2O_3 films were measured. The growth conditions and structural film properties of the high quality films have been extensively studied[16,17]. Van-der-Pauw and Hall measurements were taken on the films in a temperature range from 30 K to 300 K for film thicknesses between 28 nm to 225 nm to determine conductivity, Hall density and mobility. Besides electron-phonon and electron-ionized impurity scattering, additional scattering mechanisms for thin β-Ga_2O_3 films are discussed to explore their feasibility for future device applications. Especially, a fundamental limit due to finite size effects[18], namely the interaction of electron waves with the film boundaries, is explored.

Results

Bulk and bulk-like thick films. One unintentionally doped bulk-β-Ga_2O_3 single crystal and several Si-doped homoepitaxial layers were measured. Representative $V(I)$ and $R(B)$ curves for van-der-Pauw and Hall measurements are shown in Fig. 1. The measurement setup used here allowed a measurement accuracy of 5% for van-der-Pauw resistances and 10% for Hall resistances. The measured conductivity, Hall density, as well as the mobility of the bulk compared to a 225 nm thick homoepitaxially grown film sample are shown in Fig. 2.

The conductivity increases with increasing temperature up to a maximum of about 5 S/cm at a temperature of 150 K. For $T \gtrsim 150$ K the conductivity decreases. The Hall density increases strongly with temperature for low temperatures under 150 K. Above that, the increase of the Hall density flattens and saturates for high

[1]Novel Materials Group, Humboldt-Universität zu Berlin, Newtonstraße 15, 12489, Berlin, Germany. [2]Leibniz Institute for Crystal Growth, Max-Born-Straße 2, 12489, Berlin, Germany. Correspondence and requests for materials should be addressed to S.F.F. (email: sfischer@physik.hu-berlin.de)

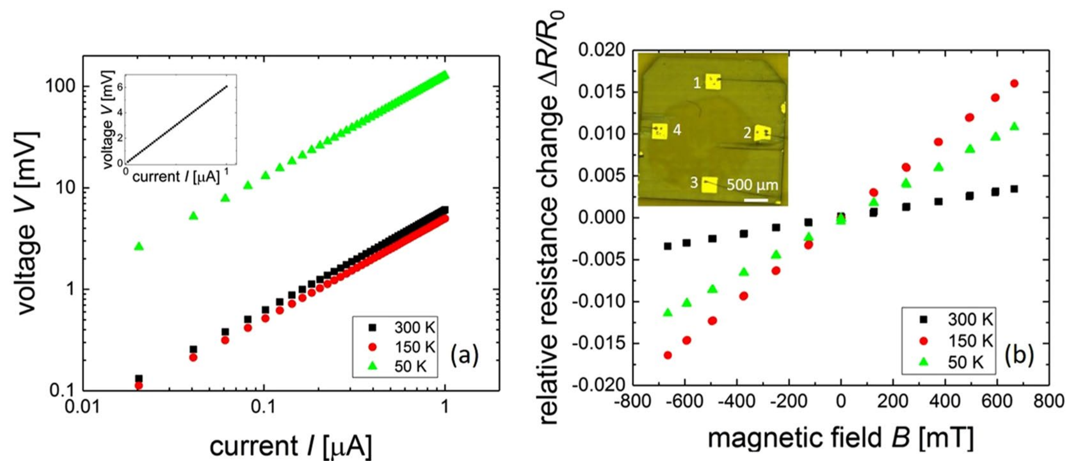

Figure 1. Representative measurement data taken at three different temperatures for (**a**) van-der-Pauw conductivity measurements, double logarithmic plot. **Inset:** linear plot of 300 K data. (**b**) Hall measurements. **Inset:** Representative sample after production of 25 nm Ti/50 nm Au contacts and bonding with Al-wire. The accuracy of the measured points is better than the size of the symbols ($\leq$1%).

temperatures. The Hall density in the film is slightly higher than the density in the undoped bulk crystal, which is expected due to the Si-doping.

Starting from low temperatures, the mobility shows a strong increase with increasing temperature until it reaches a maximum of about 550 cm^2/Vs (350 cm^2/Vs) at a temperature of 90 K for the bulk (film) sample. With a further rise in temperature, the mobility decreases. Both samples show an identical temperature dependence, however the film has a slightly lower mobility due to its higher doping level. The mobility values were fit to two dominant scattering mechanisms, ionized impurity scattering for low temperatures and optical phonon scattering for high temperatures.

Within the measurement uncertainties the samples with a 4° and 6° off-orientation of the substrate were identical. The bulk sample and the homoepitaxially-grown film are very similar, therefore the same scattering effects are to be expected in both. Since the electrical parameters of the bulk crystal compare well to the best existing literature values[12,19,20] they can serve as a reference for the following measurements on thin films.

Thick and thin films. Figure 3 shows the measured conductivities, Hall densities, as well as the mobilities of several measured thick and thin film samples. The data of the bulk crystal is also included as a reference.

Differences in conductivity and Hall density between the different samples are to be expected due to the doping range ($1 \cdot 10^{17}$–$2 \cdot 10^{18}$ cm^{-3}). With increasing doping, the donator ionization energy decreases. For higher doping about $2 \cdot 10^{18}$ cm^{-3} the sample approaches the state of a degenerate semiconductor and an almost constant temperature dependence can be observed. Fits were calculated with the charge neutrality equation, see Eq. (1). As expected, no clear trend in conductivity regarding the film thickness can be seen, however, the differences can be assigned to different doping and sample thicknesses.

The thicker films (225–155 nm) show a mobility function $\mu(T)$ that is very similar to that of the bulk crystal, with a distinct maximum between 100 K and 150 K. This maximum shifts to higher temperatures and lower mobility values if the film thickness is reduced. The absolute mobility values decrease monotonically with decreasing film thickness.

The thin films (100 nm and below) show no clear maximum in the $\mu(T)$ function. The curve shape has changed into a monotonic decrease of mobility with decreasing temperature. It should also be noted, that the absolute mobility values for the thin films below 100 nm show a drop up to two orders of magnitude whereas the film thickness only drops by one. This effect can not be ascribed to varying Hall densities. Recently, a similar mobility suppression for thin $BaSnO_3$ films was reported without a detailed analysis[21]. In the following, we discuss whether the reason for the observed mobility reduction in thin films is a result of different Hall densities, the crystal quality or the sample thickness.

Temperature Dependence of n_H and μ. Regarding the Hall densities n_H, it is shown that the $n_H(T)$ curves show the expected semiconductor-like temperature dependence, see Fig. 3b. It is fitted with the charge neutrality equation, depending on the acceptor density N_A, the donator density N_D the donator energy E_D and the effective mass m^* of the electrons

$$\frac{n(n+N_A)}{N_D - N_A - n} = N_C \exp\left(-\frac{E_D}{k_B T}\right), \tag{1}$$

with the effective density of states N_C in the conduction band being

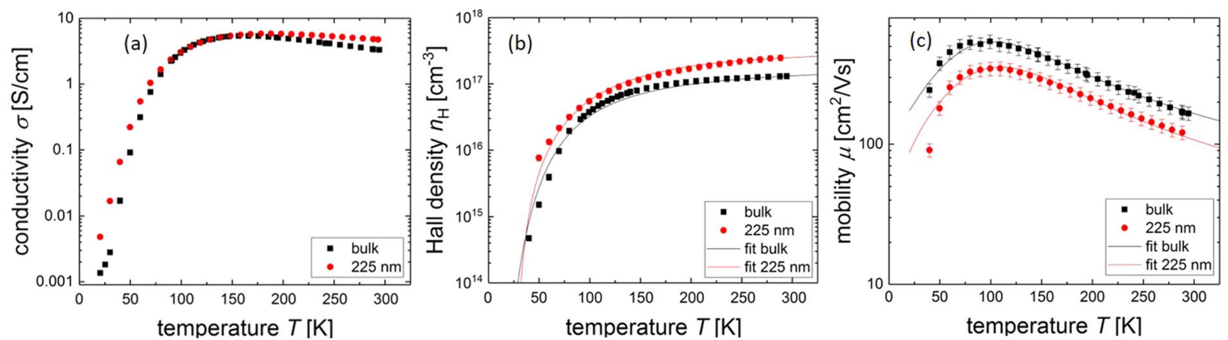

Figure 2. Summary of the reference measurements done on a not intentionally doped, (100)-orientated bulk-β-Ga_2O_3 single crystal in direct comparison to a 225 nm homoepitaxially grown Si-doped film. (**a**) Conductivity σ vs. temperature T. Both conductivites show a maximum at about 150 K. (**b**) Hall density n_H vs. temperature T. The data are fit to the charge neutrality equation (see Eq. (1)) which represents the measured data well. (**c**) Mobility μ vs. temperature T. The mobilities have been fit to two dominant scattering mechanisms: optical phonons, dominant at high temperatures and ionized impurity scattering dominant at low temperatures. Bulk and thin film mobility show a similar form. The error bars in Fig. 2c) denote the statistical and systematic error of every measuring point – following from the van der Pauw and Hall measurements (cf. Fig. 1). The solid functions were calculated with formula (7) using a least-square-fit.

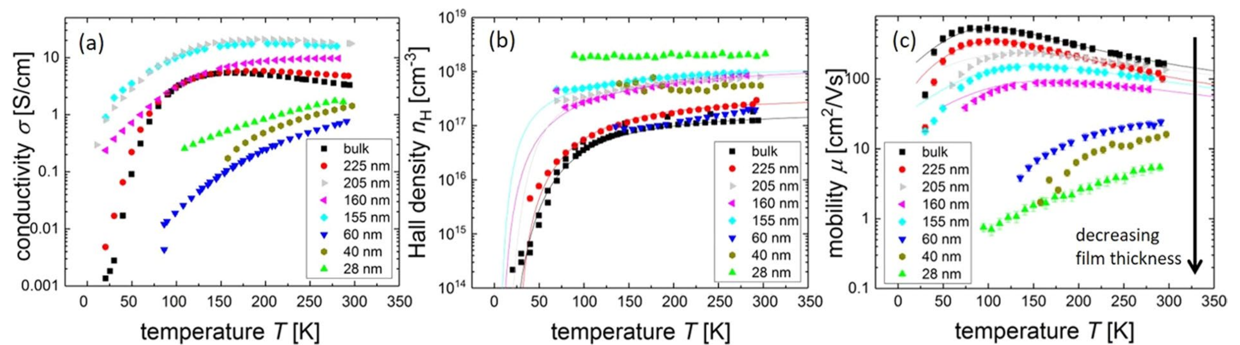

Figure 3. Summary of the measurements done on homoepitaxially grown, (100)-orientated bulk-β-Ga_2O_3 Si-doped films (doping range: $1 \cdot 10^{17}$–$2 \cdot 10^{18}\,cm^{-3}$). The solid curves are least square fits with measured values and typical material parameters (cf. Table S1). (**a**) Conductivity vs. temperature. No clear dependence on film thickness can be observed. (**b**) Hall density vs. temperature. Fits were carried out with the charge-neutrality equation. (**c**) Mobility vs. temperature. Thick films (>150 nm) show a behavior similar to the bulk, thin films (<100 nm) show a highly reduced mobility with a different temperature dependence. Note: the Hall density of the 28 nm sample was measured with the AC-Hall method, due to its low mobility. The influence of different scattering mechanisms is discussed below.

$$N_C = 2\left(\frac{m^* k_B T}{2\pi\hbar}\right)^{3/2}, \tag{2}$$

k_B as the Boltzmann constant and $\hbar$ as the reduced Planck constant. Only for the highest doped sample $n(T)$ deviates from the typical semiconductor-like temperature dependence.

Comparing the samples with a film thickness of $t = 155$ nm and $t = 28$ nm shows, that their Hall densities differ only by a factor of 2, whereas the mobility differs by almost 2 orders of magnitude. This suggests an additional scattering mechanism that relates to the sample thickness and becomes dominant in very thin films.

Regarding the mobility at high temperatures, no dependence on the film thickness is to be expected for dominating electron-phonon scattering. Figure 3c however shows, that there is a clear decrease of mobility with decreasing film thickness. This means, that an additional scattering mechanism must be a function of film thickness.

From literature[20,22–24] it is expected that scattering of electrons with optical phonons dominates the high temperature mobility behavior and scattering with ionized impurities dominates the low temperature regime. To test for that, the mobilities are fit to a model considering optical phonons and ionized impurity scattering to show the dominant scattering mechanisms. For the fit functions used here, see Suppl. Inf. S1. Both terms are independent scattering events and can therefore be added to a total mobility μ_{vol} with the Matthiessens rule[25] if lattice and electron gas are in a thermal equilibrium:

$$\frac{1}{\mu_{\mathrm{vol}}} = \frac{1}{\mu_{\mathrm{OP}}} + \frac{1}{\mu_{\mathrm{II}}}. \tag{3}$$

As shown previously for the bulk[20], ionized impurity scattering dominates the low temperature behavior of the mobility and optical phonon scattering the high temperature regime. The influence of polar optical phonons is not included in this work, since it was shown to be negligible for β-Ga_2O_3[22]. Thicker homoepitaxially grown films above 100 nm thickness show a similar temperature dependence of mobility, indicating that the same scattering mechanisms are dominant. The maximum shifts to higher temperatures and lower mobilities when reducing the film thickness.

Generally, different doping concentrations lead to different effects on the low temperature mobility due to ionized impurity scattering causing different slopes in the mobility curves for low temperatures. Possible reasons for the deviations of mobility fits from the data points for low temperatures may be neutral impurity scattering in general, growth problems at substrate/thin film interface (causing a high number of neutral impurities at the interface) or hopping transport due to impurity bands (only expected for densities above $2 \cdot 10^{18}\,\mathrm{cm}^{-3}$). Hopping has been reported to contribute to the conduction in highly doped ($4 \cdot 10^{18}\,\mathrm{cm}^{-3}$) β-Ga_2O_3 crystals for temperatures below 150 K[26]. For higher temperatures and lower doping such a contribution is not to be expected. For thinner films below 100 nm thickness, a temperature dependence of the mobility with no maximum is observed. There is a drastic reduction in mobility up to two orders of magnitude over the entire measured temperature range. This effect gets stronger with an increased reduction of film thickness. Conducting the same fits on these samples was not successful, showing that different scattering mechanisms play a role here. None of the effects mentioned above is expected to show any direct dependence on the film thickness.

Influence of Twin Boundaries. Imperfect growth may play a role for the mobility of real samples. The main type of defects in the films examined here are twin boundaries. For the purpose of calculating the scattering of electrons on those defects, the twin boundaries can be treated like grain boundaries in a polycrystalline or powdered semiconductor, with a certain potential barrier that has to be overcome[27]. Such a behavior has already been observed for homoepitaxially grown β-Ga_2O_3-films[28].

The scattering of electrons at the twin boundaries adds another term μ_{tb} to the total mobility. This term is temperature dependent and can be described as

$$\mu_{\mathrm{tb}} = \frac{eL}{\sqrt{8k_B T\pi m^*}}\exp\left(-\frac{E_B}{k_B T}\right), \tag{4}$$

where L is the mean distance between twin boundaries and E_B is the mean potential barrier height.

This model was applied to three representative thin films (28 nm, 60 nm and 155 nm) with L and E_B as fit parameters. For the 155 nm sample twin boundary scattering was added to the already described phonon and ionized impurity scattering terms, leading to corrections to the mobility fit, most clearly seen at low temperatures (as discussed in section Discussion). The two thinner films were fit only with the twin boundary model, due to the fact that phonon and ionized impurity scattering do not essentially contribute to the combined scattering. This fit yields barrier heights of around $E_B = 45$ meV for the 28 nm and 60 nm sample and about $E_B = 20$ meV for the 155 nm sample. L is calculated to be 3 nm, 15 nm and 700 nm for the 28 nm, 60 nm and 155 nm sample respectively.

For the two thinner films, the fit represents the data well, even though there are deviations for temperatures below 150 K for the 28 nm sample. However, the strong dependence of the fit parameter L on the film thickness seems unreasonable. Since the crystals defects density is not film thickness-dependent[17], a systematic reduction of the mobility due to twin boundary scattering with the film thickness is not expected. From those results we conclude that the twin boundary scattering plays only a minor role in the thicker samples. Grain boundary scattering explains a mobility reduction of films with respect to single crystalline bulk especially for low temperatures. However, it is not sufficient to explain the reduction of two orders of magnitude for thin films.

Influence of Finite Size Effects. Assuming films of high quality, possibilities for a mobility reduction in crystallographically perfect thin films are discussed in the following. Characteristic lengths that could play a role in the mobility in thin films are the effective mean free path l, the de Broglie wavelength λ_e, the sample thickness t and the surface roughness r_S.

It has been shown, that depletion due to band bending at the surface does not play a role for free standing thin β-Ga_2O_3 films[10]. However, a possibility for a mobility reduction in thin films is a surface scattering mechanism. In the semi-classical Fuchs-Sondheimer model[29–31] for ideal thin metal films the ratio of mean free path to film thickness determines the mobility. Due to the very short electron wavelengths, the situation in metals is typically $\lambda_e \ll l$ and $l \approx t$, meaning the Fuchs-Sondheimer model describes the scattering well. Furthermore, the electron wavelength is much smaller than the surface roughness $\lambda_e \ll r_S$. This leads to diffuse scattering at the surfaces. If these conditions are met, the Fuchs-Sondheimer model can also be successfully applied to thin semiconducting films[32].

However, in the semiconducting films examined here, the conditions are different: $\lambda_e > l$ and $\lambda_e \approx t$. An upper limit for l of 6 nm at RT can be estimated using the mobility value of the bulk sample (see Eq. 12). Therefore, it is much smaller than the film thickness even for the thinnest samples and highest temperatures. The scattering described by the Fuchs-Sondheimer model therefore does not play the dominant role, as shown in Suppl. Inf. S2.

Instead, the de Broglie wavelength λ_e of electrons in non-degenerate semiconductor films can be approximated by

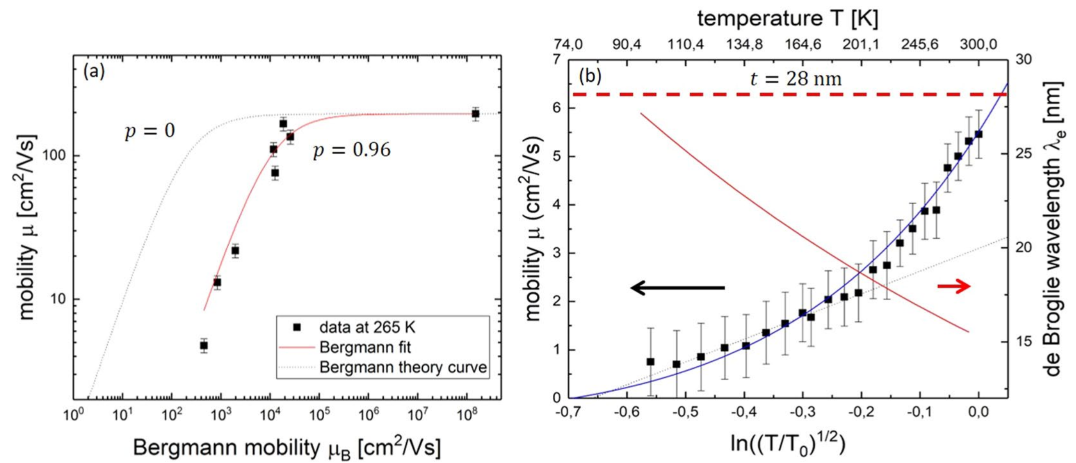

Figure 4. (**a**) Mobilities of all measured samples vs. the Bergmann mobility. The dotted black line shows the curve directly predicted by the Bergmann model, the solid red line shows a fit with a free parameter A, see Eq. (7). The fit represents the data points well, it only deviates by a constant factor of $A=0.02$. (**b**) Mobility in the 28 nm sample (left axis, black squares) and de Broglie wavelength (right axis, red line) vs. $\ln((T/T_0)^{1/2})$. The solid blue fit curve was done with Eq. (8) and shows good agreement with the data. For temperatures below 150 K, a linear fit was carried out, to show the dominance of the logarithmic $t/\lambda_{e,0}$ term. The sample thickness is marked with a thick dashed red line.

$$\lambda_e = \frac{h}{\sqrt{2m^* k_B T}}, \tag{5}$$

leading with $m^*=0.28m_0$, $T=300$ K to $\lambda_e=14$ nm. It increases for lower temperatures to tens of nm, therefore finite size effects may play a role when $\lambda_e \approx t$.

A quantum theoretical model by Bergmann[18] describes the reduction of conductivity, and hence mobility, in a crystallographically perfect thin film due to the interaction of the electron wave with the sample surface (see also Suppl. Inf. S3). As an additional scattering mechanism it adds to the total mobility the following term

$$\mu_{\text{Bergmann}} = \frac{e}{\hbar}\left(\frac{t}{\lambda_e}\right)^2 \ln\left(\frac{t}{\lambda_e}\right)\frac{1}{nt}. \tag{6}$$

It mainly depends on the ratio of film thickness t and de Broglie wavelength λ_e and has no longer any direct dependence on material parameters.

All mobility data taken at a temperature of 265 K were plotted against μ_{Bergmann} described in Eq. (6), see Fig. 4a. A fit with

$$\mu_{\text{tot}} = \left(\frac{1}{A\mu_{\text{Bergmann}}} + \frac{1}{\mu_{\text{vol}}}\right)^{-1} \tag{7}$$

was carried out. Here, μ_{vol} represents all the scattering processes that also take place in the bulk and thick film samples (see Eq. (3)) and A is a parameter, describing the deviation from the Bergmann model as described in Eq. (6).

The fit curve in Fig. 4a represents the data points well. However, it deviates from the theoretically predicted curve by a constant factor shifting it to higher values. The deviation can be described by the parameter $A=0.02$.

One explanation for this shift is the specularity parameter p. The Bergmann model was calculated from the Sondheimer model, but sets $p=0$ since it was originally developed for metals where diffusive surface scattering dominates. In Eq. (6) the sheet density nt would scale to $\frac{1+p}{1-p}nt$. For $A=0.02$ the specularity parameter must be $p=0.96$, meaning almost completely specular surface scattering. This can be explained by comparing the de Broglie wavelength in the thin films with their surface roughness. Contrary to the typical situation in metals, here it is $r_S \ll \lambda_e$. This was also confirmed by AFM measurements, where the surface roughness was determined to be below 3 nm while the de Broglie wavelength is 14 nm at 300 K. A specularity parameter close to $p=1$ indicating specular scattering is therefore reasonable.

Considering this model[18], the strongest effect is expected for the thinnest film, the 28 nm sample. The model predicts a temperature dependence of

$$\mu_{\text{Bergmann}} = \mu_0\frac{T}{T_0}\cdot\ln\left(\frac{t}{\lambda_e}\right) = \mu_0\frac{T}{T_0}\cdot\ln\left(\frac{t}{\lambda_e}\frac{\lambda_{e,0}}{\lambda_{e,0}}\right) = \mu_0\frac{T}{T_0}\left[\ln\left(\frac{t}{\lambda_{e,0}}\right) + \ln\left(\frac{\sqrt{T}}{\sqrt{T_0}}\right)\right]. \tag{8}$$

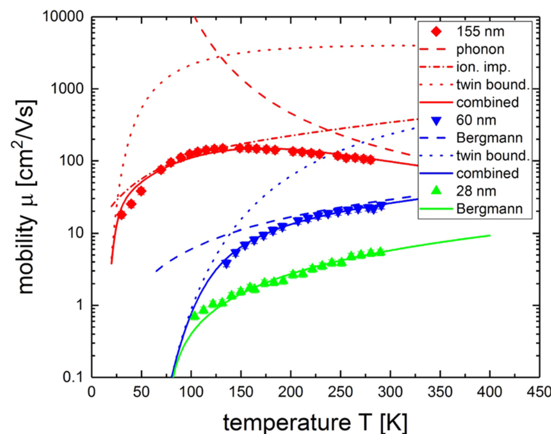

Figure 5. Mobility vs. temperature for selected samples from different thickness ranges. The plot shows an overview of the dominant scattering mechanisms in the three film thickness regimes. Phonon, ionized impurity and twin boundary scattering play a role in the thick films, twin boundary and Bergmann scattering for the intermediate films and for the thin films only the Bergmann part is dominant.

Here, $T_0 = 300$ K and $\lambda_{e,0} = 14$ nm is the corresponding de Broglie wavelength. This temperature dependence is experimentally verified for the 28 nm sample, see Fig. 4b. It is found, that $\mu_{tot} = \mu_{Bergmann}$. The data is fitted to Eq. (8) with a value of $\mu_0 = 8\frac{cm^2}{Vs}$ and shows a good agreement with the fit curve. For low temperatures (150 K and below) the data were approximated linearly to show the dominance of the logarithmic $\ln(t/\lambda_{e,0})$ term. Extrapolating the fit curve, the mobility reaches zero at about 70 K. Here, the de Broglie wavelength following Eq. (6) is $\lambda_e = 28$ nm. This is exactly the condition ($t \approx \lambda_e$) where the mobility should drop to 0 according to the Bergmann model. Generally, formula (8) approximates the measured data well.

Discussion

The previous examinations clearly show, that multiple scattering mechanisms play an important role to describe the mobility in the measured homoepitaxial thin β-Ga_2O_3 films. We identify three different thickness regimes with respect to dominance of the several scattering mechanisms: The thicker, bulk-like films (150 nm and above), an intermediate thickness range (150–50 nm) and the very thin films (50 nm and below).

For the bulk-like films, phonon scattering for high temperatures and ionized impurity scattering for low temperatures are the most dominant scattering mechanisms. The scattering at twin boundaries also gives an important correction for low temperatures. A representative fit conducted for the 155 nm sample considering these three mechanisms is shown in Fig. 5.

Both the Bergmann model[18] and the scattering on twin boundaries[27] can mathematically describe the reduction of mobility observed in the thinner films. However, a direct dependence on the film thickness is not to be expected for twin boundary scattering. The mobility reduction due to the Bergmann model clearly dominates in thinnest 28 nm sample, as seen in Fig. 5. The twin boundary scattering can not explain the low mobilities in thin films alone. A combination of these two mechanisms describes the mobility in the intermediate region between thin and thick films.

In Fig. 5 the 60 nm sample has been fitted to both of these mechanisms and reproduces the measured mobility well. The Bergmann part dominates for higher temperatures and the twin boundary scattering becomes relevant below 150 K. The fit parameters come out to be $\mu_0 = 20\frac{cm^2}{Vs}$, $L = 515$ nm and $E_B = 79$ meV. The de Broglie wavelength $\lambda_{e,0} = 14$ nm is independent of the sample thickness. Comparing this to the twin boundary scattering fit results of the 155 nm sample gives a much more consistent development of values for L, indicating that the two films are of comparable crystal quality. In the intermediate region between thin and thick films, both mechanisms are relevant and have to be considered. The amount of twin boundaries present in the crystal will determine the exact location of this intermediate region. The different barrier heights E_B can be explained by the different doping levels $N_D - N_A$, the potential decreases with $1/(N_D - N_A)$[27]. For the samples with a thickness of 155 nm and 60 nm, the data confirm this, as seen in Fig. 5. For the doping level of the thinnest 28 nm film, the twin boundary scattering plays a negligible role. The Bergmann model reproduces both the film thickness and temperature dependence of the mobility for this sample as can be seen in Figs 4 and 5. Therefore, it is considered to be the relevant scattering mechanism.

In summary, temperature and film thickness dependent measurements on homoepitaxially grown β-Ga_2O_3-films were performed in this work. A mobility comparable to bulk crystals was found in the thicker MOVPE-grown films around 200 nm film thickness. Furthermore, the measurements have shown that even the thinnest films (28 nm) have a high enough conductivity to be electrically usable at room temperature. A film thickness-dependent model for the electron mobility was discussed here, considering all dominant scattering mechanisms (optical phonon, ionized impurity, twin boundary and finite size scattering) for thick bulk-like films, intermediately thick films and thin films. It could be shown, that for the thinnest films, the defect density in the currently grown high quality crystals is not the limiting factor for the mobility. Instead, the mobility here is

limited by a finite-size effect of the films. The de Broglie wavelength in these films was found to be comparable to the film thickness. The conductivity can therefore not be described by the typically used Fuchs-Sondheimer model but by the Bergmann model. A quantitative agreement with the data can be seen, when a scaling factor assigned to the specularity parameter is taken into account. For the thicker films however, improvements in crystal growth can still lead to a rise in mobility values.

Methods

A bulk β-Ga_2O_3 single crystal as well as thin homoepitaxial layers have been examined here. Bulk β-Ga_2O_3 single crystals were grown from the melt by the Czochralski method[15,33,34] at the Leibniz Institute for Crystal Growth. For that purpose Ir crucibles with an inductive heating were used. For the present study, including substrates for homoepitaxy, 2 inch diameter crystals were obtained, which required a high oxygen concentration in a growth atmosphere (supplied in a specific way) to overcome thermodynamic limitations[34]. The crystals were either electrically insulating (doped with Mg), or semiconducting (undoped), which all were grown along the [010] crystallographic direction. Mg-doped crystals were used for off-oriented (100) substrate preparation for the growth of homoepitaxial layers. The substrate preparation was done by CrysTec GmbH, Berlin.

Thin films were grown via MOVPE[35]. Trimethylgallium and pure oxygen were used as precursors. Tetraethylorthosilicate was used as source for Si doping. The substrate temperature during deposition was kept of about 825 °C, the chamber pressure was set to 5 mbar.

The electrically insulating (100)-orientated Mg-doped β-Ga_2O_3 single crystals were used as substrate for the MOVPE growth of the electrically conducting epitaxial Si-doped β-Ga_2O_3 films, meaning the epitaxial layers were grown in (100)-orientation as well. The (100) surface of the substrates were prepared with a 4°–6° off orientation from the [100] axis in [00−1] direction to reduce island growth in the films[16]. To enhance their *n*-type semiconductor characteristics, the films were doped by silicon. Typically, the substrates/films had a size of 5 × 5 mm with film thicknesses varying between 28 nm and 225 nm.

It has been shown by AFM measurements[17] that the MOCVD grown (100) β-Ga_2O_3-films with a substrate off-orientation angle between 4° and 6° exhibit step flow growth. Also, no interface could be observed between substrate and film in TEM pictures[16], proving homoepitaxial growth. This was also confirmed by diffraction patterns. This gives reason to assume that the grown films generally are of high structural quality. If defects, mainly a low density of twin boundaries, exist, they grow through the whole film[17], meaning that there is no systematic difference between samples of different thicknesses to be expected. However, the interface between substrate and film is strongly defined by their different conductivities. The substrate is insulating whereas the film is n-conducting, leading to a potential difference at the interface.

No significant difference in sample surface roughness between the thickest (225 nm) and the thinnest measured film (28 nm) have been observed by AFM measurements. Both surfaces showed an average roughness of well below 3 nm.

Ohmic contacts on the sample were realized using aluminum (Al), gold (Au) and titanium (Ti). After cleaning the samples in acetone, a positive photoresist (AZECI 3007) was spun on to the sample at 3500 rpm for 50 s. After that, laser lithography was performed and the sample was developed in a developer solution (AZ 326 MIF). The metal contacts were then produced via magnetron sputtering of 25 nm Ti and 50 nm of Au onto the sample with subsequent liftoff in acetone in an ultrasonic bath. In a next step, the sample was glued into a chip carrier for measurements and wedge bonded with Al-wire. It should be noted, that ohmic contacts were achieved only by bonding with Al-wire, therefore point like contacts on the bonding sites can be realized.

All measurements were done in a KONTI IT™ flow cryostat. Van-der-Pauw and Hall-measurements were carried out in a temperature range between 30 K and 300 K. For the van-der-Pauw measurements, the sample is ideally contacted at four points very close to the sample edges. A current I is then applied between the two neighboring contacts (1, 2), the voltage V is measured along the other two contacts (3, 4). Doing this measurement in two alternating configurations yields two resistances ($R_{12,43}$, $R_{23,14}$), from which the conductivity σ can be determined by

$$\frac{1}{\sigma} = \frac{\pi t}{\ln(2)} \frac{R_{12,43} + R_{23,14}}{2} f, \tag{9}$$

where t is the film thickness and f is a correction factor depending on the sample shape. The deviation caused by the placement of contacts away from the sample edges leads to another correction factor, needed to calculate the correct conductivity and Hall density. Those correction factors were simulated with a finite elements simulation using the program COMSOL™.

The measurements were taken with a Keithley™ 2450 Sourcemeter, evaluating a current sweep to obtain the resistances being measured. With these measurements, conductivities and Hall carrier densities were determined. The Hall coefficient is assumed to be 1 in this work. The Hall mobility μ_H is therefore written simply as μ. The Hall density n_H can be determined, when measuring the sample in a magnetic field B perpendicular to the sample. With variations in the magnetic field ΔB, the measured resistance $R_{13,24}$ will change by ΔR and the Hall density can be calculated as

$$n_H = \frac{\Delta B}{et\Delta R}, \tag{10}$$

with e as electron charge and t as film thickness. With the conductivity σ and the Hall density the mobility μ could be calculated using

$$\mu = \frac{\sigma}{en_H}. \tag{11}$$

From the mobiities, an effective mean free path l for the carriers can be calculated as

$$l = \frac{\mu}{e}\sqrt{2m^* k_B T}, \tag{12}$$

with m^* as effective mass. For samples with very low mobilities (below 1 cm^2/Vs), an AC measurement technique was used to determine the Hall density by using periodically oscillating magnetic fields (frequency below 1 Hz). A similar approach was used for example by Chen *et al*.[36].

References

1. Stepanov, S., Nikolaev, V., Bourgrov, V. & Romanov, A. Gallium Oxide: Properties And Applications –A Review. *Rev. Adv. Master Sci.* **44**, 63–86 (2016).
2. Fortunato, E., Ginley, D., Hosono, H. & Paine, D. C. Transparent Conducting Oxides for Photovoltaics. *MRS Bull.* **32**, 242–47 (2007).
3. Marks, T. J. *et al*. Chemical and Thin-Film Strategies for New Transparent Conducting Oxides. *MRS Bull.* **25** (2000).
4. Suzuki, N. *et al*. Fabrication and characterization of transparent conductive Sn-doped β-Ga_2O_3 single crystal. *Phys. Status Solidi C* **4**, 2310–2313 (2007).
5. Tippins, H. Optical Absorption and Photoconductivity in the Band Edge of β-Ga_2O_3. *Phys. Rev.* **140**, 316–319 (1965).
6. Lorenz, M. R., Woods, J. F. & Gambino, R. J. Some electrical properties of the semiconductor β-Ga_2O_3. *J. Phys. Chem. Solids* **128**, 403–404 (1967).
7. Orita, M., Ohta, H., Hirano, M. & Hosono, H. Deep-ultraviolet transparent conductive β-Ga_2O_3 thin films. *Appl. Phys. Lett.* **77**, 4166–4168 (2000).
8. Pearton, S. J. *et al*. A review of Ga_2O_3 materials, processing, and devices. *Appl. Phys. Rev.* **5**, 011301 (2018).
9. Goldberg, Y., Levinshtein, M. E. & Rumyantsev, S. L. Properties of Advanced SemiconductorMaterials GaN, AlN, SiC, BN, SiC, SiGe (Eds Levinshtein, M. E., Rumyantsev, S. L., Shur, M. S., John Wiley & Sons, Inc., 2001).
10. Peelaers, H. & Van de Walle, C. G. Lack of quantum confinement in Ga_2O_3 nanolayers. *Phys. Rev. B* **96**, 081409 (2017).
11. An, Q. & Li, G. Shear-induced mechanical failure of β-Ga_2O_3 from quantum mechanics simulations. *Phys. Rev. B* **96**, 144113 (2017).
12. Kang, Y., Krishnaswamy, K., Peelaers, H. & de Walle, C. G. V. Fundamental limits on the electron mobility of β-Ga_2O_3. *J. Phys. Condens. Matter* **29**, 234001 (2017).
13. Mohamed, M. *et al*. The surface band structure of β-Ga_2O_3. *J. Phys. Conf. Ser.* **286**, 012027 (2011).
14. Janowitz, C. *et al*. Experimental electronic structure of In2O3 and Ga_2O_3. New J. Phys. 13, 085014.
15. Galazka, Z. *et al*. On the bulk β-Ga_2O_3 single crystals grown by the Czochralski method. *J. Cryst. Growth* **404**, 184–191 (2014).
16. Wagner, G. *et al*. Homoepitaxial growth of β-Ga_2O_3 layers by metal-organic vapor phase epitaxy. *Phys. Status Solidi A* **211**, 27–33 (2014).
17. Schewski, R. *et al*. Evolution of planar defects during homoepitaxial growth of β-Ga_2O_3 layers on (100) substrates – A quantitative model. *J. Appl. Phys.* **120**, 225308 (2016).
18. Bergmann, G. Conductance of a perfect thin film with diffuse surface scattering. *Phys. Rev. Lett.* **94**, 106801 (2005).
19. Irmscher, K., Galazka, Z., Pietsch, M., Uecker, R. & Fornari, R. Electrical properties of β-Ga_2O_3 single crystals grown by the Czochralski method. *J. Appl. Phys.* **110**, 063720 (2011).
20. Oishi, T., Koga, Y., Harada, K. & Kasu, M. High-mobility β-Ga_2O_3 (201) single crystals grown by edge-defined film-fed growth method and their Schottky barrier diodes with Ni contact. *Appl. Phys. Express* **8**, 031101 (2015).
21. Sanchela, A. V. *et al*. Large thickness dependence of the carrier mobility in a transparent oxide semiconductor, La-doped $BaSnO_3$. *Appl. Phys. Lett.* **112**, 232102 (2018).
22. Parisini, A. & Fornari, R. Analysis of the scattering mechanisms controlling electron mobility in β-Ga_2O_3 crystals. *Semicond. Sci. Technol.* **31**, 035023 (2016).
23. Ma, N. *et al*. Intrinsic electron mobility limits in β-Ga_2O_3. *Appl. Phys. Lett.* **109**, 212101 (2016).
24. Ghosh, K. & Singisetti, U. Ab initio calculation of electron–phonon coupling in monoclinic β-Ga_2O_3 crystal. *Appl. Phys. Lett.* **109**, 072102 (2016).
25. Matthiessen, A. On the Electric Conducting Power of the Metals. *Phil. Trans. R. Soc. Lond.* **148**, 383–387 (1858).
26. Oishi, T., Harada, K., Koga, Y. & Kasu, M. Conduction mechanism in highly doped β-Ga_2O_3 (201) single crystals grown by edge-defined film-fed growth method and their Schottky barrier diodes. *Jpn. J. Appl. Phys.* **55**, 030305 (2016).
27. Seto, J. Y. W. The electrical properties of polycrystalline silicon films. *J. Appl. Phys.* **46**, 5247–5254 (1975).
28. Fiedler, A. *et al*. Influence of incoherent twin boundaries on the electrical properties of β-Ga_2O_3 layers homoepitaxially grown by metal-organic vapor phase epitaxy. *J. Appl. Phys.* **122**, 165701 (2017).
29. Fuchs, K. The conductivity of thin metallic films according to the electron theory of metals. *Math. Proc. Camb. Philos. Soc.* **34**, 100–108 (1938).
30. Sondheimer, E. The mean free path of electrons in metals. *Adv. Phys.* **1**, 1–42 (1952).
31. Sondheimer, E. The mean free path of electrons in metals. *Adv. Phys.* **50**, 499–537 (2001).
32. Anderson, J. Conduction in thin semiconductor films. *Adv. Phys.* **19**, 311–338 (1970).
33. Galazka, Z. *et al*. Czochralski growth and characterization of β-Ga_2O_3 single crystals. *Cryst. Res. Technol.* **45**, 1229–1236 (2010).
34. Galazka, Z. *et al*. Scaling-Up of Bulk β-Ga_2O_3 Single Crystals by the Czochralski Method. *ECS J. Solid State Sci. Technol.* **6**, Q3007–Q3011 (2017).
35. Baldini, M. *et al*. Si- and Sn-Doped Homoepitaxial β-Ga_2O_3 Layers Grown by MOVPE on (010)-Oriented Substrates. *ECS J. Solid State Sci. Technol.* **6**, Q3040–Q3044 (2017).
36. Chen, Y., Yi, H. T. & Podzorov, V. High-Resolution ac Measurements of the Hall Effect in Organic Field-Effect Transistors. *Phys. Rev. Appl.* **5**, 034008 (2016).

Acknowledgements

This work was performed in the framework of GraFOx, a Leibniz-ScienceCampus, partially funded by the Leibniz association and by the Deutsche Forschungsgemeinschaft (FI932/10 - 1 and FI932/11 - 1). The authors would like to thank Maximilian Kockert and Robert Schewski for fruitful scientific discussions, Raimund Grünberg for technical help in MOVPE growth, and Max Pfeifer for assistance in the experimental work.

Author Contributions

Z.G. conducted the bulk crystal growth, G.W. conducted the MOVPE growth, R.A., J.B., M.H., O.C., R.M. and S.F.F. contributed to transport experiments and analyzed the data, R.A., R.M. and S.F.F. wrote the manuscript and all authors contributed to it.

Additional Information

Supplementary information accompanies this paper at https://doi.org/10.1038/s41598-019-49238-2.

Competing Interests: The authors declare no competing interests.

Publisher's note: Springer Nature remains neutral with regard to jurisdictional claims in published maps and institutional affiliations.

Open Access This article is licensed under a Creative Commons Attribution 4.0 International License, which permits use, sharing, adaptation, distribution and reproduction in any medium or format, as long as you give appropriate credit to the original author(s) and the source, provide a link to the Creative Commons license, and indicate if changes were made. The images or other third party material in this article are included in the article's Creative Commons license, unless indicated otherwise in a credit line to the material. If material is not included in the article's Creative Commons license and your intended use is not permitted by statutory regulation or exceeds the permitted use, you will need to obtain permission directly from the copyright holder. To view a copy of this license, visit http://creativecommons.org/licenses/by/4.0/.

© The Author(s) 2019